AIP | Journal of Applied Physics

Supersaturating silicon with transition metals by ion implantation and pulsed laser melting

Daniel Recht, Matthew J. Smith, Supakit Charnvanichborikarn, Joseph T. Sullivan, Mark T. Winkler et al.

Citation: J. Appl. Phys. **114**, 124903 (2013); doi: 10.1063/1.4821240
View online: http://dx.doi.org/10.1063/1.4821240
View Table of Contents: http://jap.aip.org/resource/1/JAPIAU/v114/i12
Published by the AIP Publishing LLC.

Additional information on J. Appl. Phys.

Journal Homepage: http://jap.aip.org/
Journal Information: http://jap.aip.org/about/about_the_journal
Top downloads: http://jap.aip.org/features/most_downloaded
Information for Authors: http://jap.aip.org/authors

ADVERTISEMENT

physics today

Read author interviews in Bookends

JOURNAL OF APPLIED PHYSICS **114**, 124903 (2013)

Supersaturating silicon with transition metals by ion implantation and pulsed laser melting

Daniel Recht,[1] Matthew J. Smith,[2] Supakit Charnvanichborikarn,[3] Joseph T. Sullivan,[4] Mark T. Winkler,[4,a)] Jay Mathews,[5] Jeffrey M. Warrender,[5] Tonio Buonassisi,[4] James S. Williams,[3] Silvija Gradečak,[2] and Michael J. Aziz[1]
[1]*Harvard School of Engineering and Applied Sciences, Cambridge, Massachusetts 02138, USA*
[2]*Department of Materials Science and Engineering, Massachusetts Institute of Technology, Cambridge, Massachusetts 02139, USA*
[3]*Research School of Physics and Engineering, The Australian National University, Canberra, ACT, Australia*
[4]*Department of Mechanical Engineering, Massachusetts Institute of Technology, Cambridge Massachusetts 02139, USA*
[5]*Benet Laboratories, U.S. Army ARDEC, Watervliet, New York 12189, USA*

(Received 1 July 2013; accepted 29 August 2013; published online 27 September 2013)

We investigate the possibility of creating an intermediate band semiconductor by supersaturating Si with a range of transition metals (Au, Co, Cr, Cu, Fe, Pd, Pt, W, and Zn) using ion implantation followed by pulsed laser melting (PLM). Structural characterization shows evidence of either surface segregation or cellular breakdown in all transition metals investigated, preventing the formation of high supersaturations. However, concentration-depth profiling reveals that regions of Si supersaturated with Au and Zn are formed below the regions of cellular breakdown. Fits to the concentration-depth profile are used to estimate the diffusive speeds, $v_{D,}$ of Au and Zn, and put lower bounds on v_D of the other metals ranging from 10^2 to 10^4 m/s. Knowledge of v_D is used to tailor the irradiation conditions and synthesize single-crystal Si supersaturated with 10^{19} Au/cm^3 without cellular breakdown. Values of v_D are compared to those for other elements in Si. Two independent thermophysical properties, the solute diffusivity at the melting temperature, $D_s(T_m)$, and the equilibrium partition coefficient, k_e, are shown to simultaneously affect v_D. We demonstrate a correlation between v_D and the ratio $D_s(T_m)/k_e^{0.67}$, which is exhibited for Group III, IV, and V solutes but not for the transition metals investigated. Nevertheless, comparison with experimental results suggests that $D_s(T_m)/k_e^{0.67}$ might serve as a metric for evaluating the potential to supersaturate Si with transition metals by PLM. © *2013 AIP Publishing LLC*.
[http://dx.doi.org/10.1063/1.4821240]

I. INTRODUCTION

A potential strategy for producing an intermediate band in silicon (Si) that could be useful for sub-bandgap photodetectors or photovoltaics[1,2] is to incorporate a dopant that creates a filled and an empty level near mid-gap. At sufficiently high concentrations, the two levels may overlap to form a single partially filled band. This approach necessitates multiple mid-gap levels. Transition metals could introduce such a combination of states, but are typically avoided in Si devices because they significantly reduce minority-carrier lifetime even at dilute concentrations.[3–5] To achieve the overlap, solute concentrations well beyond the equilibrium solubility limits of most solutes in Si must be achieved.[2,6,7]

When nanosecond-scale pulsed laser melting (PLM) is applied to ion-implanted Si, the ultra-fast resolidification that follows melting can produce single crystalline Si supersaturated with the implanted solute. To achieve supersaturation, the solidification speed v must be high enough, compared to the diffusive speed v_D of the solute, for deviations from local interfacial equilibrium to cause significant solute trapping.[8–11] Ion implantation and PLM have been used to synthesize single-crystalline silicon supersaturated with a range of dopants from group III–group VI and their diffusive speeds have been well characterized.[10–15] Transition metals, however, have proven challenging; early attempts at non-equilibrium doping of Si with transition metals resulted in complete segregation out of the solid during resolidification.[16–20] There have been isolated reports of supersaturated concentrations of Au (Ref. 21) and Pt (Ref. 22) achieved in Si using PLM, but uncertainty remains about the possibility of achieving supersaturated concentrations of a wider array of transition metals in silicon. Studies have also been reported of the use of pulsed melting techniques to incorporate supersaturations of Mn into Si[23,24] and Ge[25,26] in search of carrier-mediated ferromagnetism. Motivated by the potential synthesis of an intermediate band semiconductor, we set out to improve the understanding of the phenomenology and mechanisms dictating the incorporation of transition metals into silicon during the PLM process.

In this work, we investigate dopant incorporation of nine different transition metals (Au, Co, Cr, Cu, Fe, Pd, Pt, W, and Zn) ion-implanted into Si and melted and rapidly resolidified using nanosecond PLM. Using scanning electron microscopy (SEM), cross-section transmission electron microscopy (XTEM), and secondary ion mass spectrometry (SIMS), we

[a)]Present address: IBM Thomas J. Watson Research Center, Yorktown Heights, New York 10598, USA.

 © 2013 AIP Publishing LLC

fully characterize the extent of dopant incorporation, dopant segregation, and cellular breakdown. We use this information to extract estimates of or lower limits to v_D for each transition metal. These investigations inform the selection of laser irradiation conditions that lead to the successful incorporation of Au into monocrystalline Si at supersaturated concentrations. Finally, we combine our estimates (or lower limits) of v_D for transition metals with knowledge about the behavior of group III–VI solutes in silicon to elucidate the relationship between v_D and thermophysical properties of the solute. We propose and rationalize a correlation between v_D and more readily available solute properties. This correlation provides insight into the behavior of solute atoms at the solid-liquid interface and leads to a parameter that might serve as a metric for evaluating the potential for significant solute trapping of transition metals in Si.

II. EXPERIMENTAL

Si wafers ((001), p-type, 1–10 Ω-cm) were ion implanted with $^{197}Au^+$, $^{59}Co^-$, $^{52}Cr^-$, $^{63}Cu^-$, $^{56}Fe^+$, $^{184}W^+$, $^{66}Zn^-$ and the natural isotopic mixes[27] of Pd^+ and Pt^+ at the energies and doses listed in Table I. Samples were melted with one 3×3 mm^2 laser pulse at 1.7 J/cm^2 from a spatially homogenized, pulsed $XeCl^+$excimer laser (308 nm, full width at half maximum (FWHM) 25 ns, total pulse duration 50 ns) using the melting procedure described in Ref. 10. The low-dose Fe-implanted sample (1×10^{14} cm^{-2}) was pre-amorphized by Si implantation at 85 keV to a dose of 3×10^{15} cm^2.

Based on the results of this initial investigation, (001) Si (*n*-type, 5 Ω-cm) and (111) Si (p-type, 1000 Ω-cm) were implanted with $^{197}Au^-$ at 50 keV to a dose of 10^{14} cm^2 and then melted with one 3×3 mm^2 pulse at 0.6 J/cm^2 from a frequency-tripled, pulsed Nd:YAG laser (355 nm, 6 ns FWHM, 9 ns total duration, 20% spatial intensity variation) using an otherwise identical procedure. The maximum melt depths were approximately 350 nm for the $XeCl^+$excimer laser and 150 nm for the Nd:YAG laser. Simulations suggest[28] that following one $XeCl^+$ excimer laser pulse, the solidification speed peaks slightly above 5 m/s near the beginning of solidification and drops to under 3 m/s at the end of solidification; and that following a single Nd:YAG laser pulse, the solidification speed peaks at just over 10 m/s and drops to 7 m/s at the end of solidification.

The resulting microstructure of the supersaturated layers was characterized by XTEM. Concentration-depth profiles were measured by Rutherford backscattering spectrometry (RBS) with 2 MeV $^4He^+$ ions for Fe and W and by SIMS for all other elements.[29] Where possible, concentration-depth profiles from SIMS were fit using models for PLM and solute diffusion[10,12,28,30] and these fits yielded best estimates of v_D, a key parameter governing the amount of solute partitioning during rapid solidification. According to the continuous growth model for solute trapping,[9,10]

$$k = \frac{k_e + (v/v_D)}{1 + (v/v_D)}, \quad (1)$$

where k is the partition coefficient (the ratio of the solute concentration in the solid to that in the liquid at the interface), k_e is its equilibrium value, and v is the solidification speed.

TABLE I. Summary of results and key experimental quantities for Si implanted with transition metals and melted with a $XeCl^+$ excimer laser. Dose and energy refer to the implantation parameters. "Breakdown" describes whether cellular breakdown of the solidification front was observed in transmission electron micrographs (see supplementary material). c_{max} is the maximum incorporated concentration with the noise floor of SIMS or RBS used as a bound if no incorporation could be detected. v_D is the diffusive speed determined by fitting concentration-depth profiles with the model described in the text where possible (Au) and otherwise bounded using the model and instrumental bounds on c_{max} (all others). The solidification-front velocity through the part of the doping profile to which the fitting is most sensitive varied from about 4.5 to 3 m/s.

Element	Dose	Energy	Breakdown	c_{max}	v_D
Au	1×10^{16} cm^2	325 keV	Yes	5×10^{19} cm^3	350 m/s
Co	1×10^{16} cm^2	120 keV	Yes	$<10^{18}$ cm^3	$\gtrsim 10^4$ m/s
Cr	5×10^{15} cm^2	95 keV	Yes	$<10^{18}$ cm^3	$\gtrsim 10^4$ m/s
Cu	4.5×10^{15} cm^2	120 keV	No	$<10^{19}$ cm^3	$\gtrsim 10^3$ m/s
Fe	1×10^{16} cm^2	140 keV	Yes	$<10^{20}$ cm^3	$\gtrsim 10^2$ m/s
Fe	1×10^{15} cm^2	140 keV	No	$<10^{20}$ cm^3	N/A
Fe	1×10^{14} cm^2	140 keV	No	$<10^{20}$ cm^3	N/A
Pd	5.4×10^{15} cm^2	200 keV	Yes	$<5 \times 10^{19}$ cm^3	$\gtrsim 10^2$ m/s
Pt	3×10^{15} cm^2	325 keV	Yes	$<10^{19}$ cm^3	$\gtrsim 10^3$ m/s
W	1×10^{16} cm^2	180 keV	Yes	$<10^{19}$ cm^3	$\gtrsim 10^3$ m/s
Zn	5×10^{15} cm^2	120 keV	Yes	$\approx 2 \times 10^{18}$ cm^3	$\approx 10^4$ m/s

III. RESULTS

Our investigation into the behavior of nine transition metals (Au, Co, Cr, Cu, Fe, Pd, Pt, W, and Zn) following PLM using a $XeCl^+$ excimer laser is summarized in Table I. Cellular breakdown of the solidification front occurred for Au, Co, Cr, Pd, Pt, and the highest dose of Fe (1×10^{16} cm^{-2}). Lower doses of Fe (1×10^{14} cm^{-2}–1×10^{15} cm^{-2}) and Cu did not contain transition metal concentrations above the detection limit of SIMS (Cu) and RBS (Fe), suggesting surface segregation of the transition metal solutes. XTEM characterization of all the samples presented in Table I is available in the supplementary material.[31] Transition metals leading to surface segregation at low concentrations and cellular breakdown at higher concentrations, as observed here, is consistent with previous investigations into PLM of transition metals ion implanted in Si.[14,15,20,28,32,33]

As an example of typical cellular breakdown morphology, Figure 1(a) shows a SEM micrograph of the sample implanted with 10^{16} $^{56}Fe^+$ cm^2 and then laser-melted. The XTEM micrograph in Figure 1(b) shows solute-rich walls between cells of the host semiconductor, the signature feature of cellular breakdown. The spacing between cell walls, as visible in Figure 1(b) and the supplementary material,[31] is on the order of D_L/v, where D_L is the solute diffusivity in the liquid. The high density of cell walls prevents the determination of the level of dopant incorporation in the crystalline Si grains (i.e., between the cell walls) using SIMS. Accordingly, the values of or bounds on the maximum trapped solute concentration, c_{max}, reported in Table I are based on the maximum

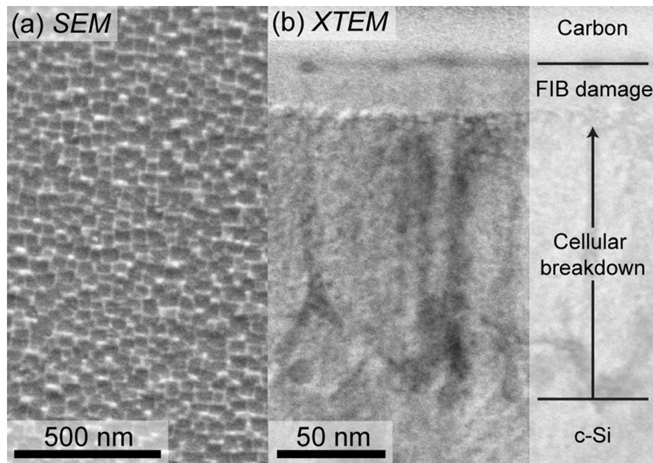

FIG. 1. (a) Plan-view SEM and (b) XTEM images of Si implanted with $^{56}Fe^{+}$ at $10^{16}\,cm^{-2}$ and melted with a $XeCl^{+}$ excimer laser. The cell walls visible in both images are clear evidence of cellular breakdown of the solidification front. The cross section reveals that cell walls extend to a depth of roughly 150 nm, which is less than the melt depth (~350 nm) and enables estimation of the lower limit of the diffusive speed.

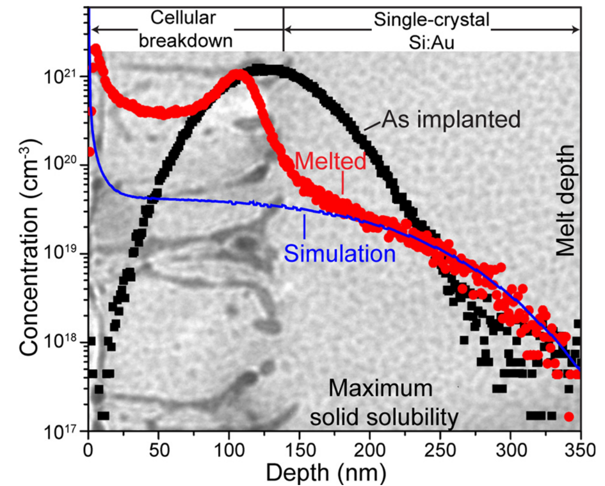

FIG. 2. Concentration-depth profile and XTEM image of Si implanted with $^{197}Au^{-}$ to a dosage of $10^{16}\,cm^{-2}$ (black) and melted (red) with a $XeCl^{+}$ excimer laser. Au is trapped in single-crystal Si at concentrations up to $5\times10^{19}\,cm^{2}$, more than two orders of magnitude above the solid solubility limit, before the onset of breakdown. The subsurface peak in concentration at the boundary of a region of elevated concentration reflects cell-wall impurity enrichment that was common to all samples in which breakdown occurred. A simulation fit (blue) was performed over depths below the onset of cellular breakdown for the melted sample, as described in the text. Additional contrast in the single-crystal region of the XTEM image is due to ion-beam damage during XTEM sample preparation.

concentration of the solute in monocrystalline silicon below the breakdown region. Because we are modeling large supersaturations, k_e is assumed to be negligible compared to unity when modeling dopant diffusion and segregation using Eq. (1).

We interpret the observed difficulty of incorporating high non-equilibrium concentrations of low-k_e transition metals into Si to be a consequence of the large v_D exhibited by the transition metals in comparison with conventional Si dopants. Large values of v_D cause a spike in solute concentration in the liquid at the solidification front due to strong solute partitioning at the liquid-solid interface, and this build-up of solute increases the probability of cellular breakdown, a morphological instability in which local freezing-point depression due to solute partitioning causes runaway amplification of small perturbations to the solidification front, leading to a cellular microstructure. In most samples studied, the diffusive speed was large enough that c_{max} was below the detection limit of the concentration-depth profiling measurements. The values or lower limits of v_D determined here for Au, Co, Cr, Cu, Fe, Pd, Pt, W, and Zn are at least an order of magnitude larger than values of v_D previously reported for group III–VI elements in Si during PLM.[12–15] Although v_D has not been explicitly reported previously, these results are consistent with previous investigations into PLM of Si implanted with transition metals.[16–18,20] The values of k reported are consistent with the upper limits previously reported[34] for transition metals in Si ($k < 10^{-2}$) and agree with previously reported values[21] for Au in Si.

As presented in Table I, the Au concentration was well above $10^{19}/cm^{3}$, Zn was detectable slightly above the SIMS noise floor of $10^{18}\,cm^{3}$, and both are at least an order of magnitude higher than the solubility of Au in Si ($4.8\times10^{16}\,cm^{-3}$ at 1100 °C)[35] and Zn in Si ($1.1\times10^{17}\,cm^{-3}$ at 1211 °C).[36] Though the Zn concentration profile[31] approached the SIMS noise floor, the data still allowed us to estimate v_D. Figure 2 shows a XTEM image overlaid on a concentration-depth profile of the Au-doped sample described in Table I, illustrating that a supersaturated layer with thickness > 100 nm formed below the depth at which cellular breakdown began.

The Au concentration-depth profile for the supersaturated layer was fit using the simulation described in Refs. 10, 12, and 30 in order to extract v_D and D_L. Fitting the data in Figure 2 yields $D_L = 4.5\times10^{-4}\,cm^{2}/s$ and $v_D = 350\,m/s$. Using these parameters in steady-state interface stability theory,[28] we calculated the critical solute concentration for the stability of a liquid-solid interface traveling at 3 m/s, and found that a concentration of Au in the bulk liquid greater than $1.2\times10^{18}\,cm^{-3}$ results in an unstable interface. However, if the velocity is increased to 7 m/s, the interface is stable for concentrations up to $9\times10^{18}\,cm^{-3}$.[28] Using thermal conditions from one-dimensional heat flow simulations, we find, in rough agreement with the data, that the solidification front under our experimental excimer laser PLM conditions should become unstable at a depth of about 250 nm and thus that cellular breakdown should subsequently become observable at some shallower depth. Further, modeling of interface stability and of the onset of breakdown after an interface becomes unstable is underway.

Based on our understanding of v_D for Au in Si, a preliminary effort was made to produce a breakdown-free sample of Si containing even more Au by increasing the solidification speed in order to suppress solute segregation. To obtain an increased speed, the laser pulse duration was reduced by a factor of ten (by using a different, Nd:YAG-based laser) and the implant and melt depths were decreased by more than a factor of two, as explained in the experimental section. Both of these changes reduce the total thermal input into the sample, which results in a sharper temperature gradient during resolidification and a faster dissipation of heat from the melt to the underlying solid substrate. Both (001) and (111) Si

were tested because v_D is known to be significantly smaller in (111) Si (i.e., more conducive to solute trapping) than in other orientations.[11]

Figure 3(a) shows XTEM images of the (001) and (111) samples implanted with Au and melted with the Nd:YAG laser. Whereas the (001) sample was found by XTEM to be single-crystalline and free of defects, stacking faults are clearly visible in the (111) sample. The formation of stacking faults during the rapid solidification of (111) Si is a well-known phenomenon at high solidification speeds.[37,38] Figure 3(b) plots the concentration-depth profiles and the associated simulation fits for PLM using the Nd:YAG laser on both (001) and (111) Si:Au. These fits yielded a value for D_L in good agreement with the previous experiments ($D_L = 4.5 \times 10^{-4}$ cm^2/s) but a good fit could not be obtained for the (001) data using the v_D estimated for the XeCl$^+$ irradiated sample ($v_D = 350$ m/s). The best fit was instead achieved with $v_D = 110$ m/s. This discrepancy appears to be too large to be explained by measurement error alone. Though it could be an artifact of differences in the background doping or laser pulse spatial and temporal profiles, this discrepancy may indicate that, although k increases with v for Au in Si(001), the partitioning behavior is not well described by Eq. (1).

Fitting the depth profile for the (111) sample using Eq. (1) under the assumption that the influence of stacking faults on SIMS is negligible yields $v_D = 30$ m/s. Inserting this value of v_D and the simulated solidification velocities into Eq. (1) indicates that the partition coefficient for (111) is 0.23–0.33. This is three times higher than the value for (001) of 0.06–0.09, as is consistent with results for other dopants in Si.[11]

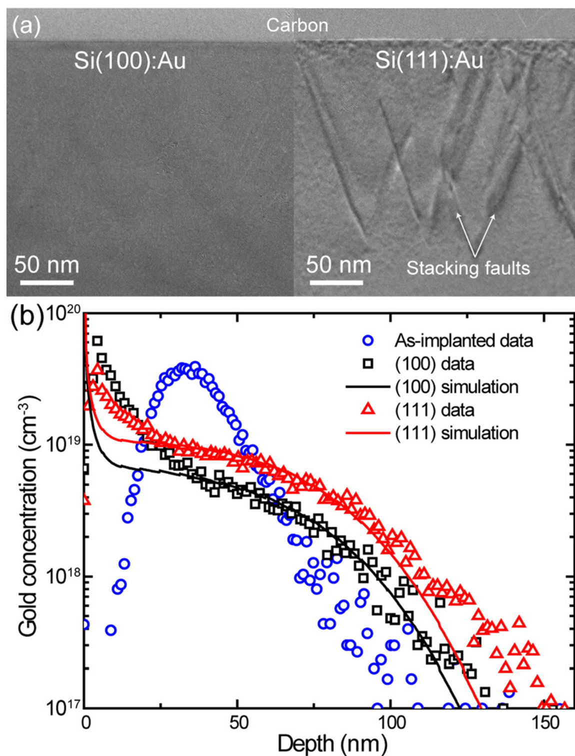

FIG. 3. (a) XTEM images of (001) Si and (111) Si implanted with 50 keV ^{197}Au$^-$ to the dose of 10^{14} cm^2 and melted with an Nd:YAG laser as described in the text. The (001) Si is single-crystal and without extended defects, whereas the (111) Si exhibits stacking faults. (b) Concentration-depth profiles and associated simulation fits for (001) and (111) Si:Au. The surface concentration peak is likely a signal from the Au segregated to the surface and broadened by the SIMS instrument.

Figure 3 shows that we synthesized an approximately 100-nm thick layer of single-crystal (001) Si that is free of extended defects and supersaturated with Au to a concentration of roughly 10^{19} cm^{-3}, which is two orders of magnitude above the solid solubility limit. The relatively low diffusive speed of Au in Si is fortuitous, as Au impurities are known to create the filled and empty midgap energy levels required for the formation of a useful intermediate band.[3] In principle, observing band-like conduction in the states induced by Au requires a solute concentration above both the threshold for impurity-state delocalization and the threshold concentration for overlap between the filled and empty impurity levels. One estimate[39] suggests that elements such as Au, which create states near mid-gap in Si, should undergo a Mott insulator-to-metal transition at a concentration of approximately 6×10^{19} cm^{-3}.[40] However, this is likely to be an underestimate as the experimental thresholds[7,41] for S and Se are above 10^{20} cm^{-3} and, because Au creates a deeper level than does S or Se, its critical concentration would likely be higher. Considering both the substantial reduction in dopant segregation observed in the Nd:YAG melted samples relative to the XeCl$^+$ melted sample and previous demonstrations of Au supersaturation in Si,[21] it may be possible to increase the concentration of Au further without inducing cellular breakdown merely by increasing the implant dose. For $v_D = 110$ m/s and assuming steady-state solidification conditions, we predict fully stable solidification at 6×10^{19} cm^{-3} if the solidification speed exceeds 7 m/s, which is achievable with the Nd:YAG laser used here.

IV. DISCUSSION

There has been interest in understanding how v_D relates to more readily measured thermophysical properties of the alloy system, both for predicting the v_D of untested materials and for elucidating the kinetics of solute trapping at the resolidification front.[11,17,19,42,43] To gain insight into these relationships, here we compare the v_D of transition metals in Si (or their lower limits), determined in this work, with previously reported values for a wide range of solutes.

The diffusive speed is related[8] to the diffusivity of the impurity at the interface, D_i, and the distance between atomic sites, λ, by $v_D = D_i/\lambda$. With little information about D_i, correlations have been examined between v_D and the diffusivity of the impurity in crystalline silicon at the Si melting point ($D_s(T_m)$).[17,42] We plot v_D vs. $D_s(T_m)$ for 16 solutes in Fig. 4(a). A strong positive correlation between the two properties is apparent. It has been suggested that D_i can be approximated as the geometric mean of the diffusivity in molten silicon and crystalline Si at the melt temperature ($D_i = \sqrt{D_S(T_M)D_L}$).[42] However, there is only 15% variation in D_L across all solutes presented here, and we find that taking the geometric mean of $D_s(T_m)$ and D_L does not improve on the correlation between v_D and $D_s(T_m)$.

We also observe a strong inverse correlation between v_D and the equilibrium partition coefficient, k_e, as shown in

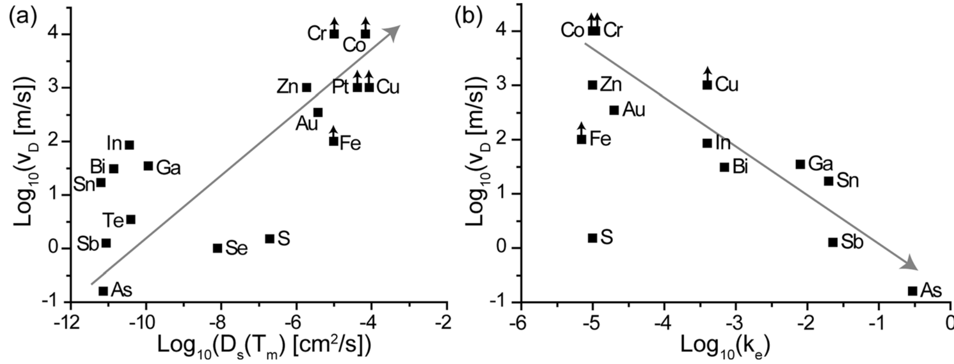

FIG. 4. Correlations between the (001) diffusive speed, v_D, and (a) the diffusivity in crystalline silicon at T_m (1687 K), $D_s(T_m)$, and (b) the equilibrium partition coefficient, k_e. Values or lower limits for v_D of Au, Co, Cr, Cu, Fe, Pd, Pt, W, and Zn were determined in this work. Values of v_D were collected from the following sources: As, Bi, Ga, In, and Sb were reported in Ref. 11, Sn in Ref. 26 and S, Se, and Te in Ref. 12. Values for $D_s(T_m)$ are calculated from values reported in: As, Bi, Sb, Ga, and In,[53] Au and Zn,[54] Co,[55] Cr,[56] Cu,[57] Fe,[58] Pt,[59] S,[60] Se,[61] Sn,[47] and Te.[62] Values for k_e are values reported in: As, Bi, Cu, Ga, In, Sb, and Zn,[17] Au,[21] Co and Cr,[63] Fe,[64] S,[65] and Sn.[66] Pt, Se, and Te are omitted from (b) due to lack of available information.

Fig. 4(b). This correlation has been previously rationalized[11,43] as a consequence of an energy barrier for solute redistribution that varies with the energetic component of the thermodynamic driving force within the context of the continuous growth model,[5] as shown in Fig. 5. The rate at which a solute makes thermally activated transitions from a state of high redistribution potential in the crystal at the interface (state A) to an adjacent state of low potential in the melt (state B) is governed by the height of the activation barrier (state A*). The redistribution potential, μ', is the chemical potential of the solute minus the contribution from the ideal configurational entropy of mixing.[9] Uniformity of chemical potential in equilibrium requires

$$k = \exp\left(\frac{\Delta\mu'}{RT}\right), \tag{2}$$

where $\Delta\mu'$ is the difference between μ' in the solid and that in the liquid, and R is the universal gas constant. We seek a correlation among many different impurities in silicon, each of which has its own barrier height and its own value of $\Delta\mu'$.

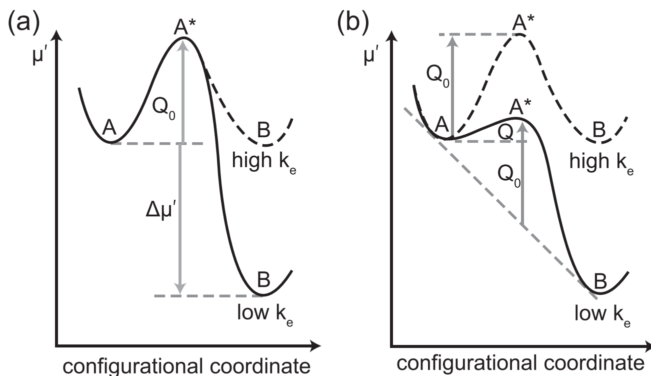

FIG. 5. (a) Reaction coordinate diagram for thermally activated escape of solute from high-potential position in solid at interface to low-potential position in melt. Solid curve represents a low-k_e solute and dashed curve represents a high-k_e solute. In (a), the activation barrier remains a fixed height Q_0 above the initial state A, corresponding to Eq. (3) with $\alpha = 0$. In (b), the barrier remains a fixed height Q_0 above the average value of the initial state A and the final state B, corresponding to Eq. (3) with $\alpha = 1/2$. After Refs. 11 and 43.

Redistribution potential landscapes for two such impurities are sketched in Fig. 5: the solid curves represent a low-solubility impurity, and the dashed curves represent a high-solubility impurity. A proportionality has been proposed[11,43] between the amount the barrier height Q drops and the relative amount the potential well in the liquid drops as one considers impurities of progressively decreasing k_e (increasingly more negative values of $\Delta\mu'$)

$$Q = Q_D + \alpha\Delta\mu', \tag{3}$$

where α is the correlation coefficient. Fig. 5(a) illustrates the case $\alpha = 0$ (barrier height with respect to state A is independent of $\Delta\mu'$) and Fig. 5(b) illustrates the case $\alpha = 1/2$ (barrier height drops half as much as does state B, with respect to state A). Early studies[11,43] found $\alpha \approx 0.6$. The diffusive speed itself is related to the barrier height as a thermally activated process

$$v_D = \text{const.}\exp\left(-\frac{Q}{RT}\right). \tag{4}$$

In this work, we are concerned only with thermophysical parameters near the pure Si melting point T_m and so we replace T by T_m in Eq. (4). Likewise, the solid diffusivity is related to its apparent activation energy Q_D by

$$D_S(T_m) = D_0 \exp\left(\frac{Q_D}{RT_m}\right). \tag{5}$$

We make the approximation that the barrier height in the absence of driving force, Q_0 in Fig. 5, is approximately the apparent activation energy for diffusion in the solid, Q_D

$$Q_0 \approx Q_D. \tag{6}$$

This is certainly an oversimplification. The variation in D_0 is ignored, and Q_D contains contributions both from the point defect formation energy and the migration energy. The large number of impurity species we examine diffuse by a variety of mechanisms,[44,45] some of which change with temperature and some of which are unknown at the melting point. Hence

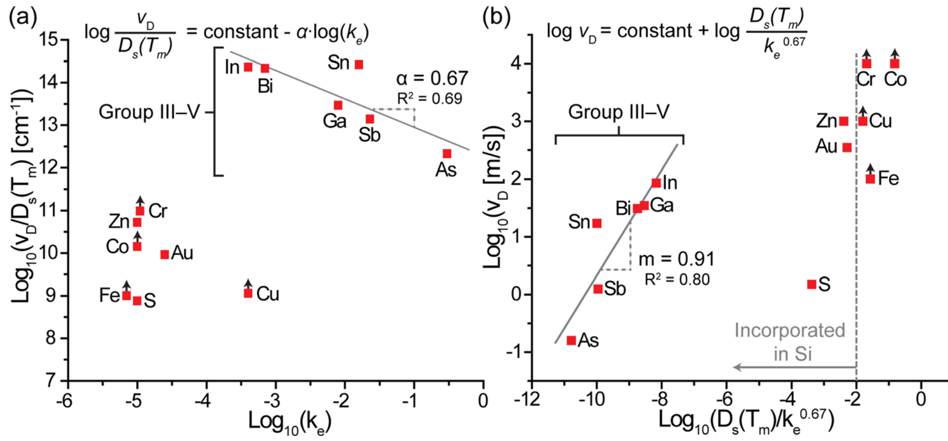

FIG. 6. (a) Log-scale scatter plot of $v_D/D_s(T_m)$ *vs.* k_e, as suggested by Eq. (8). Group III–V solutes exhibit a linear trend (solid line) with a best-fit slope (-α) of -0.67 ($R^2 = 0.69$). (b) Log-scale scatter plot v_D *vs.* $D_s(T_m)/k_e^{\alpha}$, as suggested by Eq. (7), with $\alpha = 0.67$. A linear fit to the Group III–V solutes (As, Sb, Sn, Bi, Ga, In) yields a slope m = 0.91 ($R^2 = 0.80$), in good agreement with the slope predicted (m = 1). Data presented in (a) and (b) were calculated from references listed in Figure 4. Elements for which k_e is unavailable (Pd, Pt, Se, Te) were omitted from this analysis.

we propose this simple approximation recognizing that it may fail to correlate species with different diffusion mechanisms.

A relationship between two independent thermophysical properties ($D_s(T_m)$, k_e) and v_D can be derived by combining Eqs. (2)–(6), yielding

$$\log v_D = \text{constant} + \log\left(\frac{D_S T_m}{k_e^{\alpha}}\right). \tag{7}$$

The assumptions discussed above thus lead to the prediction that a scatter plot of $\log(D_s(T_m)/(k_e^{\alpha}))$ vs. $\log(v_D)$ for solutes in Si should exhibit a correlation with a slope near unity.

To test this proposal, we first determine the best-fit value of α by rearranging Eq. (7) to read

$$\log\left(\frac{v_D}{D_S T_m}\right) = \text{constant} - \alpha \log(k_e) \tag{8}$$

and applying a linear fit to extract the slope, -α. The scatter plot suggested by Eq. (8) is shown in Fig. 6(a). In this plot, the solutes exhibit two distinct behaviors depending on their dominant diffusion mechanisms in crystalline Si. The group III, IV, and V solutes (As, Bi, Ga, In, Sb, and Sn) exhibit a much lower $D_s(T_m)$, which is a consequence of their vacancy-mediated diffusive mechanisms in c-Si.[44,46–48] These relatively slow diffusers exhibit a linear trend as predicted by Eq. (8); yielding a best-fit $\alpha = 0.67$. This value is in reasonable agreement with previous observations of the correlation between the equilibrium segregation coefficient and the diffusive velocity.[11,43] The transition metals and S, however, exhibit much higher $D_s(T_m)$ and their behavior is vastly different and apparently uncorrelated.

With a best-fit value for α established, we examine the new proposed correlation by presenting in Fig. 6(b) the scatter plot suggested by Eq. (7). The best-fit slope of the group III–V solutes, when $\alpha = 0.67$, is $m = 0.91$ ($R^2 = 0.80$), which is in good agreement with the relationship ($m = 1$) predicted by Eq. (7). This result supports the proposed correlation for the group III–V solutes in Si.

In both Figs. 6(a) and 6(b), the transition metals (Au, Co, Cr, Cu, Fe, and Zn) and S fall orders of magnitude off the linear trends exhibited by the group III–V solutes. These solutes exhibit a much higher $D_s(T_m)$ (Fig. 4(a)), which reflects their interstitial-mediated diffusion mechanisms (see references in caption of Fig. 4). It is difficult to comment with more detail on potential correlations or the applicability of Eq. (8) among the fast diffusers because most of the values determined for v_D are lower limits. We were able to obtain approximate values of v_D for Zn and Au using PLM, but there is no framework through which to interpret these values other than that they are lower than for the other transition metals. Nevertheless, Fig. 6(b) suggests that the combination $D_s(T_m)/(k_e^{0.67})$ could serve as a metric for evaluating the potential for supersaturating Si even with transition metals. Empirically, we observe measurable solute incorporation under our PLM conditions for all solutes for which $D_s(T_m)/(k_e^{0.67}) \leq 0.01\ \text{cm}^2/\text{s}$. This is the approximate value that distinguishes between the fast diffusers that were successfully incorporated into Si (S, Au, and Zn) and the transition metals that we were unable to incorporate into single crystalline Si under these irradiation conditions (Fe, Cu, Co, and Cr). Note that no such distinction can be pointed out in Fig. 6(a). For example, the $D_s(T_m)/(k_e^{0.67})$ analysis can be used to evaluate the potential supersaturation of Si with Mn, a materials system of interest for dilute magnetic semiconductors.[49,50] Utilizing values for $D_s(T_m)$ and k_e available in the literature,[51,52] we find that $D_s(T_m)/(k_e^{0.67}) = 0.03$ for Mn in Si. This is above the empirically defined threshold of 0.01, suggesting that supersaturated concentrations of Mn in Si will not form using PLM under these irradiation conditions. This is consistent with the findings of pulsed melting studies reported to date.[23,24]

V. SUMMARY

In search of a solute for the formation of an impurity band in the band gap of Si, we investigated the supersaturation of Si with transition metals using ion implantation and pulsed laser irradiation, structurally characterized the resulting material using SIMS and XTEM, and extracted v_D from the composition-depth profiles. Very large v_D (10^2–10^4 m/s) resulted in cellular breakdown at the solidification front for most transition metals. SIMS and XTEM characterization showed that both Au and Zn were incorporated into Si at high concentrations, but it was not immediately clear why these transition metals were incorporated whereas others exhibited cellular breakdown. Next, we identified strong correlations between v_D and two independent thermophysical

properties: $D_s(T_m)$ and k_e. These independent trends were consolidated into a single correlation parameter by assuming the barrier height for unbiased thermally activated jumps across the crystal-melt interface is the same as the apparent activation energy for solid-state diffusion at the melting point. The resulting correlation, described by Eq. (7) and Figs. 6(a) and 6(b), is established only for solutes that exhibit vacancy-mediated diffusion. Nevertheless, the combination $D_s(T_m)/k_e^{0.67}$ might serve as a metric for evaluating the potential for supersaturating Si with transition metals using PLM.

ACKNOWLEDGMENTS

We acknowledge H. Efstathiadis and K. Agbodo for performing Au implantations, and A. J. Akey for helpful discussions. Research at Harvard was supported by The U.S. Army Research Office under contracts W911NF-12-1-0196 and W911NF-09-1-0118. M.T.W. and T.B.'s work was supported by the U.S. Army Research Laboratory and the U.S. Army Research Office under Grant No. W911NF-10-1-0442, and the National Science Foundation (NSF) Faculty Early Career Development Program ECCS-1150878 (to T.B.). M.J.S., J.T.S., M.T.W., T.B., and S.G. acknowledge a generous gift from the Chesonis Family Foundation and support in part by the National Science Foundation (NSF) and the Department of Energy (DOE) under NSF CA No. EEC-1041895. S.C. and J.S.W.'s work was supported by The Australian Research Council. J.M. was supported by a National Research Council Research Associateship. This work was performed in part at Harvard University's Center for Nanoscale Systems, a member of the National Nanotechnology Infrastructure Network, which is supported by the NSF under Award ECS-0335765, and also made valuable use of MIT CMSE Shared Experimental Facilities, under MIT NSF MRSEC Grant # DMR-08-19762.

[1]A. Luque and A. Martí, Phys. Rev. Lett. **78**(26), 5014 (1997).
[2]A. Luque and A. Martí, Adv. Mater. **22**(2), 160 (2010).
[3]K. Graff, *Metal Impurities in Silicon-Device Fabrication* (Springer, Berlin, 2000).
[4]R. N. Hall, Phys. Rev. **87**(2), 387 (1952).
[5]W. Shockley and W. T. Read, Jr., Phys. Rev. **87**(5), 835 (1952).
[6]E. Ertekin, M. Winkler, D. Recht, A. Said, M. Aziz, T. Buonassisi, and J. Grossman, Phys. Rev. Lett. **108**, 026401 (2012).
[7]M. Winkler, D. Recht, M. Sher, A. Said, E. Mazur, and M. Aziz, Phys. Rev. Lett. **106**(17), 178701 (2011).
[8]M. J. Aziz, J. Appl. Phys. **53**(2), 1158 (1982).
[9]M. J. Aziz and T. Kaplan, Acta Metall. **36**(8), 2335 (1988).
[10]J. A. Kittl, P. G. Sanders, M. J. Aziz, D. P. Brunco, and M. O. Thompson, Acta Mater. **48**(20), 4797 (2000).
[11]R. Reitano, P. M. Smith, and M. J. Aziz, J. Appl. Phys. **76**(3), 1518 (1994).
[12]B. P. Bob, A. Kohno, S. Charnvanichborikarn, J. M. Warrender, I. Umezu, M. Tabbal, J. S. Williams, and M. J. Aziz, J. Appl. Phys. **107**(12), 123506 (2010).
[13]L. M. Goldman and M. J. Aziz, J. Mater. Res. **2**(4), 524 (1987).
[14]J. Narayan, J. Appl. Phys. **52**(3), 1289 (1981).
[15]J. Narayan, J. Cryst. Growth **59**(3), 583 (1982).
[16]P. Baeri, S. U. Campisano, G. Foti, and E. Rimini, Phys. Rev. Lett. **41**(18), 1246 (1978).
[17]S. U. Campisano and P. Baeri, Appl. Phys. Lett. **42**(12), 1023 (1983).
[18]A. G. Cullis, in *Laser Annealing of Semiconductors*, edited by J. M. Poate and J. W. Mayer (Academic Press, 1982).
[19]C. W. White, B. R. Appleton, and S. R. Wilson, in *Laser Annealing of Semiconductors*, edited by J. M. Poate and J. W. Mayer (Academic Press, 1982).
[20]C. W. White, H. Naramoto, J. M. Williams, J. Narayan, B. R. Appleton, and S. R. Wilson, MRS Proc. **4**, 241 (1981).
[21]F. Priolo, J. M. Poate, D. C. Jacobson, J. L. Batstone, J. S. Custer, and M. O. Thompson, Appl. Phys. Lett. **53**(25), 2486 (1988).
[22]A. G. Cullis, H. C. Webber, J. M. Poate, and A. L. Simons, Appl. Phys. Lett. **36**(4), 320 (1980).
[23]N. Peng, C. Jeynes, M. J. Bailey, D. Adikaari, V. Stolojan, and R. P. Webb, Nucl. Instrum. Methods B **267**(8–9), 1623 (2009).
[24]Z. Werner, C. Pochrybniak, M. Barlak, J. Gosk, J. Szczytko, A. Twardowski, and A. Siwek, Vacuum **89**(89), 113 (2013).
[25]M. C. Dolph, T. Kim, W. Yin, D. Recht, W. Fan, J. Yu, M. J. Aziz, J. Lu, and S. A. Wolf, J. Appl. Phys. **109**(9), 093917 (2011).
[26]S. Zhou, D. Burger, W. Skorupa, P. Oesterlin, M. Helm, and H. Schmidt, Appl. Phys. Lett. **96**(20), 202105 (2010).
[27]A combination of low negative ion yields and the difficulty of mass selection at large masses motivated the experimental decision to use the natural range of masses for platinum and palladium.
[28]D. E. Hoglund, M. O. Thompson, and M. J. Aziz, Phys. Rev. B **58**(1), 189 (1998).
[29]The atomic mass of Fe (56) prevents its detection in SIMS since it is obscured by the signal from the di-Si ion with the same mass. W concentration was measured by RBS as a matter of convenience.
[30]D. Recht, J. Sullivan, R. Reedy, T. Buonassisi, and M. Aziz, Appl. Phys. Lett. **100**(11), 112112 (2012).
[31]See supplementary material as http://dx.doi.org/10.1063/1.4821240 for XTEM characterization and for Zn SIMS concentration profile.
[32]A. G. Cullis, D. T. J. Hurle, H. C. Webber, N. G. Chew, J. M. Poate, P. Baeri, and G. Foti, Appl. Phys. Lett. **38**(8), 642 (1981).
[33]D. E. Hoglund, M. J. Aziz, S. R. Stiffler, M. O. Thompson, J. Y. Tsao, and P. S. Peercy, J. Cryst. Growth **109**(1–4), 107 (1991).
[34]C. W. White, B. R. Appleton, B. Stritzker, D. M. Zehner, and S. R. Wilson, MRS Proc. **1**, 59 (1980).
[35]N. A. Stolwijk, B. Schuster, and J. Hölzl, Appl. Phys. A **33**(2), 133 (1984).
[36]D. Grünebaum, T. H. Czekalla, N. A. Stolwijk, H. Mehrer, I. Yonenaga, and K. Sumino, Appl. Phys. A **53**(1), 65 (1991).
[37]A. G. Cullis, H. C. Webber, N. G. Chew, J. M. Poate, and P. Baeri, Phys. Rev. Lett. **49**(3), 219 (1982).
[38]G. Foti, E. Rimini, W. S. Tseng, and J. W. Mayer, Appl. Phys. **15**(4), 365 (1978).
[39]A. Luque, A. Martí, E. Antolin, and C. Tablero, Physica B **382**(1), 320 (2006).
[40]Metal-like conduction through the cell walls may be possible and, anecdotally, we saw some signs of this for a few samples. Accordingly, we strongly recommend using a sample, which has not broken down when evaluating the conductivity of the hyperdoped material.
[41]E. Ertekin, M. T. Winkler, D. Recht, A. J. Said, M. J. Aziz, T. Buonassisi, and J. C. Grossman, Phys. Rev. Lett. **108**(2), 026401 (2012).
[42]S. U. Campisano, G. Foti, P. Baeri, M. G. Grimaldi, and E. Rimini, Appl. Phys. Lett. **37**(8), 719 (1980).
[43]P. M. Smith and M. J. Aziz, Acta Metall. Mater. **42**(10), 3515 (1994).
[44]P. M. Fahey, P. B. Griffin, and J. D. Plummer, Rev. Mod. Phys. **61**(2), 289 (1989).
[45]U. Gösele, W. Frank, and A. Seeger, Appl. Phys. **23**(4), 361 (1980).
[46]D. A. Antoniadis and I. Moskowitz, J. Appl. Phys. **53**(12), 9214 (1982).
[47]P. Kringhøj and A. N. Larsen, Phys. Rev. B **56**(11), 6396 (1997).
[48]A. Ural, P. B. Griffin, and J. D. Plummer, J. Appl. Phys. **85**(9), 6440 (1999).
[49]M. Bolduc, C. Awo-Affouda, A. Stollenwerk, M. B. Huang, F. G. Ramos, G. Agnello, and V. P. LaBella, Phys. Rev. B **71**(3), 033302 (2005).
[50]F. J. Rueß, M. El Kazzi, L. Czornomaz, P. Mensch, M. Hopstaken, and A. Fuhrer, Appl. Phys. Lett. **102**(8), 082101 (2013).
[51]D. Gilles, W. Bergholz, and W. Schroter, J. Appl. Phys. **59**(10), 3590 (1986).
[52]E. Weber, Appl. Phys. A **30**(1), 1 (1983).
[53]C. S. Fuller and J. A. Ditzenberger, J. Appl. Phys. **27**(5), 544 (1956).
[54]H. Bracht and H. Overhof, Phys. Status Solidi A **158**(1), 47 (1996).
[55]J. Utzig and D. Gilles, Mater. Sci. Forum **38–41**, 729 (1989).
[56]N. T. Bendik, V. S. Garnyk, and L. S. Milevskii, Sov. Phys. Solid State **12**, 150 (1970).
[57]A. A. Istratov, C. Flink, H. Hieslmair, E. R. Weber, and T. Heiser, Phys. Rev. Lett. **81**(6), 1243 (1998).

[58]A. A. Istratov, H. Hieslmair, and E. R. Weber, Appl. Phys. A **69**, 13 (1999).
[59]R. F. Bailey and T. G. Mills, *Semiconductor Silicon* (The Electrochem. Soc. Inc., New York, N. Y., 1969), p. 481.
[60]F. Rollert, N. A. Stolwijk, and H. Mehrer, Appl. Phys. Lett. **63**(4), 506 (1993).
[61]H. R. Vydyanath, J. S. Lorenzo, and F. A. Kroger, J. Appl. Phys. **49**(12), 5928 (1978).
[62]F. Rollert, N. A. Stolwijk, and H. Mehrer, Mater. Sci. Eng., B **18**(2), 107 (1993).
[63]J. R. Davis, Jr., A. Rohatgi, R. H. Hopkins, P. D. Blais, P. Rai-Choudhury, J. R. McCormick, and H. C. Mollenkopf, IEEE Trans. Electron Devices **27**, 677 (1980).
[64]N. Wiehl, U. Herpers, and E. Weber, J. Radioanal. Chem. **72**, 69 (1982).
[65]S. Fischler, J. Appl. Phys. **33**(4), 1615 (1962).
[66]J. A. Burton, Physica **20**(7–12), 845 (1954).